Slender origami with complex 3D folding shapes

S. Kamrava[1], R. Ghosh[2], Y. Yang[1] and A. Vaziri[1]

[1] *Department of Mechanical and Industrial Engineering, Northeastern University - Boston, MA 02115, USA*
[2] *Department of Mechanical and Aerospace Engineering, University of Central Florida - Orlando, FL 32816, USA*

Abstract – One-dimensional slender bodies can be deformed or shaped into spatially complex curves relatively easily due to their inherent compliance. However, traditional methods of fabricating complex spatial shapes are cumbersome, prone to error accumulation and not amenable to elegant programmability. In this letter, we introduce a one-dimensional origami based on attaching Miura-ori that can fold into various programmed two- or three-dimensional shapes. We study the out-of-plane displacement characteristics of this origami and demonstrate with examples, design of slender bodies that conform to programmed complex spatial curves. Our study provides a new, accurate, and single actuation solution of shape programmability.

The inherent compliance of slender structures makes them easy to deform into complex spatial shapes. This makes them the geometry of choice for a number of biological applications such as DNA scaffolds [1–4], microbial appendages [5–7] and plant tendrils [8]. Many engineering designs also seek to leverage this deformability in applications such as robotic grippers [9–12], deployable structures [13–16], medical implants [17,18], prosthetics [19] and soft robotics [20,21]. However, biological structures still show far greater shape flexibility, functionality and deformation rates, transitioning between multiple shapes over wide time scales from fast protein folding that takes few microseconds [22] to very slow movements in kingdom plantae [23]. Extracting such wide range of responses has been challenging for man-made structures. However, ability to attain complex geometries is highly desirable since it leads to an expansion of the design space and functionality. Typically one can obtain complex spatial curves either through direct fabrication using conventional manufacturing such as wire draw and metal forming or modern additive manufacturing. These are difficult to adapt for complicated spatial curves due to complexity of the fabrication setup for the conventional process and the complexity of scaffolds, overhangs and sensitivity to process parameters for additive manufacturing.

A typical alternative is to start from an easily available thin flat sheet and then crimp it repeatedly to obtain the desired shape. Figure 1(a) shows a simple example of such a geometry which can be obtained from a straight reference configuration of a slender metallic plate. In this case, multiple crimps (localized bending) were used to shape the straight metallic plate into the desired eight-pointed-star–like shape. While such localized bending and twisting can be used to form a wide range of shapes, this process, like the ones mentioned earlier, is not reversible due to plastic deformation at the folds and may cause fracture [24,25]. In addition, from a fabrication standpoint, this is a multi-step process with multiple sequential crimping operations. This can lead to cumulative addition of deviations from the desired shape (increasing error). In contrast, a single-step fabrication technique in which the structure is created by a single actuation event (mechanical, chemical, thermal, etc.) is beneficial in terms of accuracy, speed and simplicity. However, a single-step crimping would require the use of specific die configurations considerably restricting its generality. On the other hand, shape memory alloys can be programmed into an initial desired shape, which would then be restored through heat [26] in a single step. However, programming the shape memory material into complex shapes would require specific molds and chips to align with the desired configuration and considerable thermal loads. Both of these processes are therefore, very difficult to scale and adapt for spatial curves. In contrast, a folding-based approach such as origami where only the fold is made of actuating/stimuli
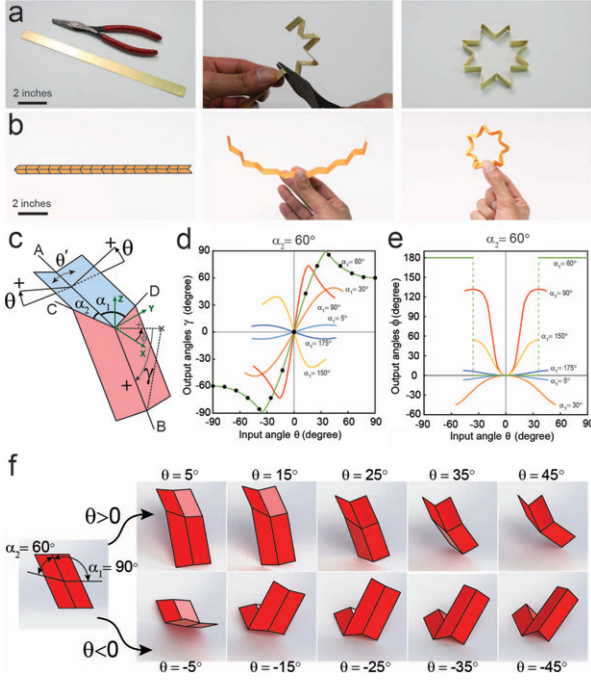
Fig. 1: (Colour online) (a) Shaping a metal strip into an eight-pointed–star shape through a sequential crimping. (b) A one-dimensional origami that evolves into an eight-pointed–star shape as it folds. (c) In the four-crease pattern, A and B creases are aligned with the longitudinal direction of the origami and creases C and D intersect with crease A with angles α_1 and α_2, respectively. (d), (e): folding response of a four-crease pattern. γ is the angle between crease B and plane XY and angle ϕ represents the out-of-plane angle of the origami and is the angle between the projection of line B on the plane XY and the X-axis. The markers on the γ plot show the analytical results for $\alpha_1 = \alpha_2 = 60°$. (f) Folding sequence of a four-crease origami with $\alpha_1 = 90°$ and $\alpha_2 = 60°$. The first row shows a valley folding ($\theta > 0°$) and the second row shows a mountain folding ($\theta < 0°$).

responsive material can enable a wide range of shapes and patterns using a single actuation event much more conveniently [27,28].

In this letter, we introduce a one-dimensional slender origami based on attaching Miura-ori [29] folds to form a slender body which can fold from a flat reference state into various programmed shapes which could be two- or three-dimensional as desired. Figure 1(b) shows an example of such one-dimensional slender origami made out of paper, which evolves into the eight-pointed–star based on a single folding action. The distinction from the crimping technique is clear in this case, because, the origami, which has one degree of freedom and a single folding action controls the global shape.

To understand the folding of such slender origami into complex shapes, we study the folding response of the Miura-ori fold shown in fig. 1(c) in which angles α_1 and α_2 are not necessarily equal. Angle θ represents the origami folding angle and varies from $0°$ (flat configuration) to the maximum possible value of $90°$ (fully folded configuration

admissible for a pattern with $\alpha_1 = \alpha_2$), see fig. 1(c). The angle $\theta = \frac{1}{2}(180° - \theta')$, where θ' is the dihedral angle between two facets sharing a longitudinal crease line (A or B). A fixed right-handed Cartesian coordinate system is attached to the origami structure with origin located on the intersection of crease lines. In our analysis, the X-axis is aligned with the crease line A and the Z-axis is the bisector of the angle θ'. Angle γ is measured between the XY plane and the crease line B and can vary from $-90°$ to $90°$ during the folding of the origami structure with the positive direction convention shown in the figure. The angle ϕ is the angle between the X-axis and the projection of crease B on the XY plane. This angle can vary from $-180°$ to $180°$ with the positive direction convention shown in the figure. The Miura-ori, also known as four-crease pattern, has only one degree of freedom [30]. Therefore, its configuration at any arbitrary folding level can be fully defined by either γ, ϕ or θ.

The relationship between θ and γ or θ and ϕ is highly non-linear and there are no available analytical solutions for them. However, some numerical approaches or restricted analytical solutions for the case of $\alpha_1 = \alpha_2$ are available [12,31–33]. We simulated the folding of origami in a commercially available software, SolidWorks (Dassault Systems, Vlizy-Villacoublay, France). The simulations solve the rigid-body equations of motion for each origami facet numerically to predict geometrically admissible configurations [34]. These simulations estimate the relation between angle θ and output parameters γ and ϕ as the origami folds. Figure 1(d) shows the dependence of γ on θ when $\alpha_2 = 60°$ and α_1 varies from $5°$ to $175°$. γ starts from $0°$ at $\theta = 0°$ and as the value of θ approaches $+90°$ or $-90°$, γ goes back to zero after passing through an extremum point. The folding procedure stops at a folding angle corresponding to the contact between facets. This maximum value of θ can be determined as a function of α_1 and α_2 (see Supplementary Material `Supplementarymaterial.pdf` for the derivation of this equation),

$$\theta_{max} = \pm\left(90° - \frac{1}{2}\cos^{-1}\left(\frac{\tan\alpha_2}{\tan\alpha_1}\right)\right), \qquad (1)$$

where $|\tan\alpha_1| > |\tan\alpha_2|$. We can compare our numerical simulations with the special case of $\alpha_1 = \alpha_2 = \alpha$ for which a closed-form solution for γ as a function of θ is available in the literature [12],

see eq. (2) on the next page

where $k = 1$ for $\theta \geq 0°$ and $k = -1$ for $\theta < 0°$. Note that from eq. (1), in this case, contact would occur only when $\theta = \pm90°$ which is the fully folded state. This is an important practical case for flat folding design. The black markers on the $\alpha_1 = \alpha_2 = 60°$ curve, in fig. 1(d) indicate the analytical results obtained from eq. (2), which shows an excellent agreement with simulations. Interestingly, fig. 1(d) also shows that the angle γ is an odd

$$\gamma = \begin{cases} 2k\cos^{-1}\left(\dfrac{\cos\alpha}{\sqrt{1-\cos^2\theta\sin^2\alpha}}\right), & \text{for } \theta \le \cos^{-1}(\sqrt{1-\cot^2\alpha}), \\[3mm] 2\pi - 2k\cos^{-1}\left(\dfrac{\cos\alpha}{\sqrt{1-\cos^2\theta\sin^2\alpha}}\right), & \text{for } \theta > \cos^{-1}(\sqrt{1-\cot^2\alpha}), \end{cases} \tag{2}$$

function of θ. Physically this indicates that reversing the sign of θ (folding in opposite direction) merely changes the direction but keeps the absolute value of γ constant. Figure 1(e) shows the corresponding variation of the angle ϕ with θ. This figure shows that as the origami folding proceeds (increasing the absolute value of θ), ϕ also increases from zero. It subsequently achieves an extremum value, which corresponds to the maximum twisting of the Miura-ori and eventually ends at a non-zero value of ϕ at θ_{max} due to contact. In contrast to γ, ϕ is an even function of θ, which means that the direction of folding is immaterial to both the direction and magnitude of ϕ. These mathematical outcomes are illustrated in fig. 1(f), which is a set of illustrations from folding of four-crease pattern with $\alpha_1 = 90°$ and $\alpha_2 = 60°$ in both directions ($\pm\theta$). The value of γ is positive when it folds downward and negative when it folds upward, and regardless of the folding direction, line B turns toward the larger angle α, which satisfies the properties expected of an even function in fig. 1(e). Four-crease patterns with different α_1 and α_2 and lengths can be attached together along a straight line to form a slender origami that could fold to a wide range of programmed two-dimensional and three-dimensional shapes.

Next, we study the out-of-plane displacement of a slender origami, which is critical for creating three-dimensional folding shapes because a design with only in-plane displacement would only fold into planar shapes. We consider a slender origami with length L and width W, which comprises six four-crease patterns with underlying angles $\alpha_1 = 90°$, $\alpha_2 = 60°$, $\alpha_1' = 90°$ and $\alpha_2' = 120°$, fig. 2(a). We quantify this out-of-plane displacement (OPD), as the distance between the free end of the string and the XZ plane of the first four-crease pattern in the string. The number of segments along a slender origami is denoted by n and is equal to the number of four-crease patterns plus one. Angles α_1, α_2, and n are considered as the three main characteristics of the presented origami, which can be altered to change the OPD of the string. Figure 2(b) shows the value of $\frac{OPD}{L}$, which is a dimensionless parameter, as a function of θ (folding level) for different n values, while θ varies from the initial folding angle $0°$ to the maximum folding angle $45°$ determined from eq. (1). For $n = 1$, normalized OPD is always zero by definition but for larger n, it always starts from zero and goes to some non-zero value. For $n = 2$, normalized OPD increases almost linearly with θ. However, as the number of unit cells increases, such linear and monotonic behavior should not be expected. This is because the position of the free end (tip) of the origami is determined by the complex interaction of rotations of individual units. This would mean that for a given configuration and
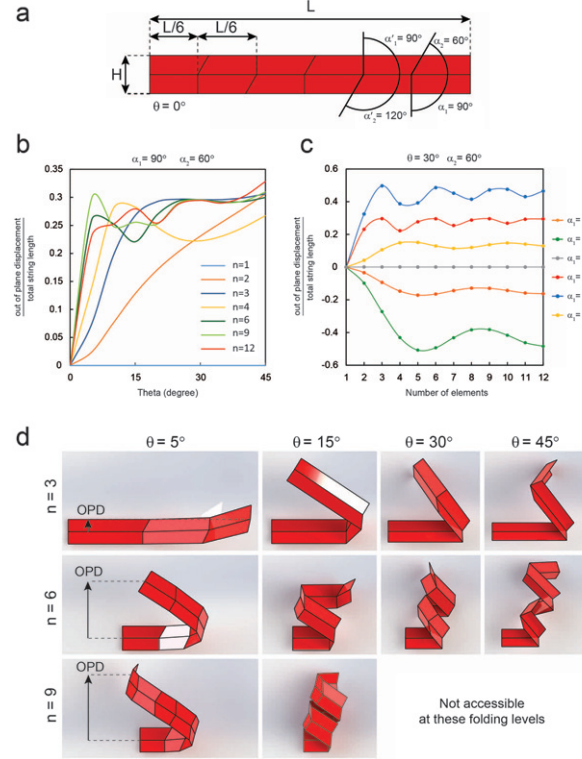

Fig. 2: (Colour online) Out-of-plane displacement of origami string. (a) Origami string made from five interconnected four-crease patterns in a $L \times W$ paper strip with repetitive $\alpha_1 = 90°$, $\alpha_2 = 60°$ and their supplementary angles. (b) Simulation results for the variation of normalized out-of-plane displacement (OPD) as a function of angle θ for different numbers of segments (n). (c) Simulation results for the variation of normalized OPD as a function of n for different angles α. (d) Three origami strings with equal lengths (l) and 3, 6 and 9 number of segments at four levels of folding ($\theta = 5°$, $15°$, $30°$ and $45°$). The folded configurations for a string with nine divisions and $\theta > 21°$ is not accessible due to the self-intersecting in string.

folding level of an origami, simply increasing the number of units would not necessarily lead to increase in OPD. This is shown in fig. 2(c) where we study the variation of normalized OPD in a folded string ($\theta = 30°$) with different angles α_1 with $\alpha_2 = 60°$ as a function of n. The figure shows that for any configuration, the origami with more elements correspond to an increasing OPD magnitude for the initial addition of units. However, the increase is not monotonic as the complexity of the origami increases with units. These mathematical insights are summarized pictorially in fig. 2(d) which illustrates the change of OPD during the folding for three strings with n equal to 3, 6 and 9 (angles α_1 and α_2 are the same as in fig. 2(a)) in four
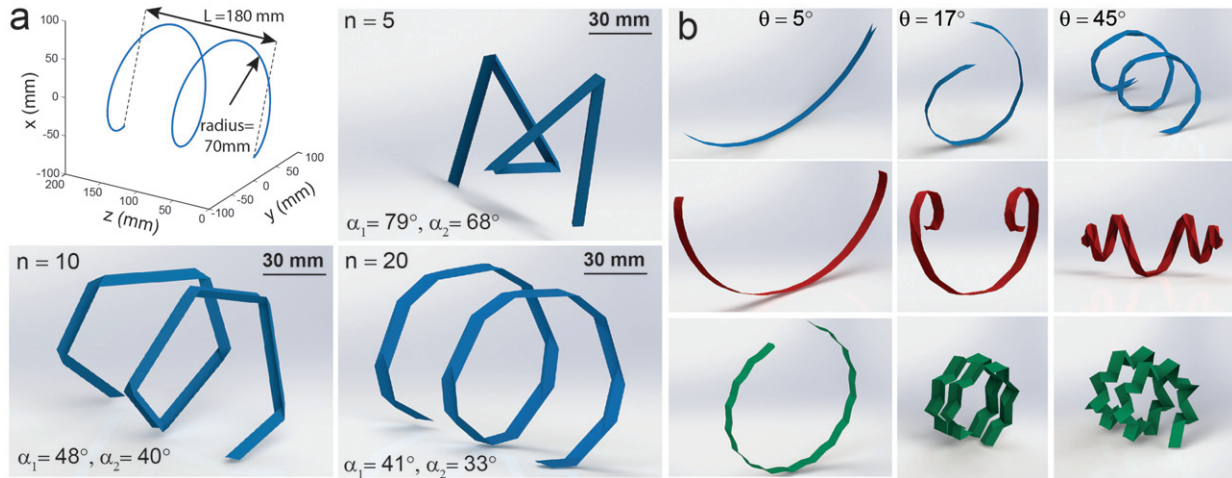
Fig. 3: (Colour online) Designing a 3D string. (a) A helix with equation $x(z)^2 + y(z)^2 = 70^2$ is discretized to n (5, 10, and 20) equal segments. The corresponding angles of γ and ϕ are measured between each two neighboring segments and then values of α_1 and α_2 are chosen based on the measured values of γ and ϕ. Three origami strings with 5, 10 and 20 segments are shown here which fit to the helix curve with some amount of error and as n increases this error diminishes. (b) Three strips of paper with identical length and width are patterned by different crease line. Three folding levels ($\theta = 5°, 17°$ and $45°$) are shown for each design. Blue, red and green strings fold to a helical, double-spiral and star-helical final shapes at $\theta = 45°$, respectively.

levels of folding. The inflections in tip deflections observed in fig. 2(b), (c) can be seen in the changing tip positions with folding level in this figure. The figure also shows that the number of origami units cannot be increased unencumbered since self-contact prevents access to the maximum possible folding range, limiting the design space.

Our study so far has shown that using Miura-ori units, the tip of the structure can be raised to a programmed spatial position. However, the real strength of the method comes from an extension of this technique to synthesize more complex spatial curves. We illustrate this by designing an origami, which folds into a helix described by $x = -70\cos(\frac{\pi z}{45})$ mm and $y = 70\sin(\frac{\pi z}{45})$ mm, where $0 \le z \le 180$ mm, as shown in fig. 3(a). This is a helix of radius 70 mm and pitch 90 mm. To design the origami to approximate this helix, we divide the helix into $n+1$ equal segments by putting n markers in equal distances along the helix. This means that the coordinates of each marker can be obtained from plugging $z_i = i\frac{L}{n}$ into the X and Y expression of the helix equation, where $i = 0, 1, \ldots, n$ representing the i-th marker. Thus, the helix is now divided into $n + 1$ nodes. Adjacent nodes can be connected by straight line segments leading to n straight line segments. We then treat each pair of adjacent lines as part of a four-crease origami. In this construction, the origin of our coordinate system introduced earlier will be at the intersection of these pairs of lines and we will measure the γ and ϕ angles between them. The angles γ, ϕ are determined from the geometry of the line segments. Using simulations, we can choose appropriate α_1 and α_2 which would be the best approximation for γ and ϕ of a particular four-crease pattern. The angles α_1 and α_2 do not have to be unique for this design of the helix but would determine the crease pattern along the helix. As the

number of line segments approximating the helix increases, the changes in γ would be milder giving rise to smoother and better approximations. However, at the same time there is an inherent limit on the number of segments due to self-contact of the origami. Figure 3(a) shows three designed origamis with $n = 5, 10$, and 20 which mimic the given helix. As expected, when n is increased, the origami better approximates the helix while folding. The values of α_1 and α_2 repeating along the entire slender origami are shown in the bottom left corner of each picture.

The same procedure can be implemented to design origami, which fold to other more complex shapes from a flat reference state which can serve applications such as robotic manipulator [12,35], deployable space structures [36] and foldable building blocks [37]. In fig. 3(b), we illustrate the folding procedure of three examples including helix, double-spiral, and star-shape helix with identical unfolded shape and completely different folded configurations.

In conclusion, our work provides an alternative to design 3D space curves out of a flat and thin sheet to other techniques such as discretized rigid-foldable curvatures [38], continues buckled curvature [39,40] and tessellated origami patterns to approximate a 3D geometry [28]. However, this method is distinct in providing a simple way to fabricate spatial shapes using a single actuation regardless of the complexity of the desired pattern. This technique overcomes many of the limitations of traditional fabrication techniques.

$* * *$

REFERENCES

[1] HAN DONGRAN, PAL SUCHETAN, NANGREAVE JEANETTE, DENG ZHENGTAO, LIU YAN and YAN HAO, *Science*, **332** (2011) 342.

[2] HANNESTAD JONAS K., SANDIN PETER and ALBINSSON BO, *J. Am. Chem. Soc.*, **130** (2008) 15889.

[3] KE YONGGANG, ONG LUVENA L., SHIH WILLIAM M. and YIN PENG, *Science*, **338** (2012) 1177.

[4] ROTHEMUND PAUL W. K., *Nature*, **440** (2006) 297.

[5] BRENNEN CHRISTOPHER and WINET HOWARD, *Annu. Rev. Fluid Mech.*, **9** (1977) 339.

[6] BLOCKER ARIEL, KOMORIYA KAORU and AIZAWA SHIN-ICHI, *Proc. Natl. Acad. Sci. U.S.A.*, **100** (2003) 3027.

[7] GHOSH RANAJAY, KUMAR ALOKE and VAZIRI ASHKAN, *PLoS ONE*, **9** (2014) e114613.

[8] GORIELY ALAIN and TABOR MICHAEL, *Phys. Rev. Lett.*, **80** (1998) 1564.

[9] AMASE HIDEYUKI, NISHIOKA YASUTAKA and YASUDA TOSHIHIKO, *Mechanism and basic characteristics of a helical inflatable gripper,* in *2015 IEEE International Conference on Mechatronics and Automation (ICMA)* (IEEE) 2015, pp. 2559–2564.

[10] VOISEMBERT SEBASTIEN, RIWAN ALAIN, MECHBAL NAZIH and BARRACO ANDRÉ, *A novel inflatable robot with constant and continuous volume,* in *2011 IEEE International Conference on Robotics and Automation (ICRA)* (IEEE) 2011, pp. 5843–5848.

[11] NISHIOKA YASUTAKA, UESU MEGUMI, TSUBOI HISAE and KAWAMURA SADAO, *Proposal of an extremely lightweight soft actuator using plastic films with a pleated structure,* in *2012 19th International Conference on Mechatronics and Machine Vision in Practice (M2VIP)* (IEEE) 2012, pp. 474–479.

[12] KAMRAVA SOROUSH, MOUSANEZHAD DAVOOD, FELTON SAMUEL M. and VAZIRI ASHKAN, *Adv. Mater. Technol.*, **3** (2018) 1700276.

[13] PUIG L., BARTON A. and RANDO N., *Acta Astronaut.*, **67** (2010) 12.

[14] HANAOR A. and LEVY R., *Int. J. Space Struct.*, **16** (2001) 211.

[15] KAMRAVA SOROUSH, GHOSH RANAJAY, WANG ZHIHAO and VAZIRI ASHKAN, to be published in *Adv. Eng. Mater.* (2018) 1800895.

[16] KAMRAVA SOROUSH, *Origami-Based Structure with Programmable Properties*, Order No. 10624068 Northeastern University, 2017, Ann Arbor: *ProQuest*. Web 12 Dec. 2018.

[17] PARYAB NASIM, CRONIN DUANE, LEE-SULLIVAN PEARL, YING XIONG, BOEY FREDDY Y. C. and VENKATRAMAN SUBBU, *J. Med. Devices*, **6** (2012) 021012.

[18] STOECKEL D., BONSIGNORE C. and DUDA S., *Minim. Invasive Ther. Allied Technol.*, **11** (2002) 137.

[19] WEYAND PETER G., BUNDLE MATTHEW W., MCGOWAN CRAIG P., GRABOWSKI ALENA, BROWN MARY BETH, KRAM RODGER and HERR HUGH, *J. Appl. Physiol.*, **107** (2009) 903.

[20] RAFSANJANI AHMAD, ZHANG YUEROU, LIU BANGYUAN, RUBINSTEIN SHMUEL M. and BERTOLDI KATIA, *Sci. Robot.*, **3** (2018) eaar7555.

[21] CONNOLLY FIONNUALA, WALSH CONOR J. and BERTOLDI KATIA, *Proc. Natl. Acad. Sci. U.S.A.*, **114** (2017) 51.

[22] KUBELKA JAN, HOFRICHTER JAMES and EATON WILLIAM A., *Curr. Opin. Struct. Biol.*, **14** (2004) 76.

[23] FORTERRE YOËL, *J. Exp. Bot.*, **64** (2013) 4745.

[24] VALIEV R. Z., ALEXANDROV I. V., ZHU Y. T. and LOWE T. C., *J. Mater. Res.*, **17** (2002) 5.

[25] VALIEV RUSLAN, *Nat. Mater.*, **3** (2004) 511.

[26] FUNAKUBO HIROYASU and KENNEDY J. B., *Shape Memory Alloys* (Gordon and Breach) 1987.

[27] OVERVELDE JOHANNES T. B., DE JONG TWAN A., SHEVCHENKO YANINA, BECERRA SERGIO A., WHITESIDES GEORGE M., WEAVER JAMES C., HOBERMAN CHUCK and BERTOLDI KATIA, *Nat. Commun.*, **7** (2016) 10929.

[28] DUDTE LEVI H., VOUGA ETIENNE, TACHI TOMOHIRO and MAHADEVAN L., *Nat. Mater.*, **15** (2016) 583.

[29] MIURA K., *Method of Packaging and Deployment of Large Membranes in Space, International Astronautical Federation*, Paper IAF-80-A31, Tokyo, Japan, 1980.

[30] KAMRAVA SOROUSH, MOUSANEZHAD DAVOOD, EBRAHIMI HAMID, GHOSH RANAJAY and VAZIRI ASHKAN, *Sci. Rep.*, **7** (2017) 46046.

[31] HULL THOMAS C. *et al.*, *Linear Algebra Appl.*, **348** (2002) 273.

[32] HUFFMAN DAVID A., *IEEE Trans. Comput.*, **10** (1976) 1010.

[33] WU WEINA and YOU ZHONG, *Proc. R. Soc. A: Math. Phys. Eng. Sci.*, **466** (2010) 2155.

[34] C SOLIDWORKS, *Understanding motion simulation*, 2010.

[35] EDMONDSON BRYCE J., BOWEN LANDEN A., GRAMES CLAYTON L., MAGLEBY SPENCER P., HOWELL LARRY L. and BATEMAN TERRI C., *Oriceps: Origami-inspired forceps,* in *ASME 2013 Conference on Smart Materials, Adaptive Structures and Intelligent Systems* (American Society of Mechanical Engineers) 2013, p. V001T01A027.

[36] ZIRBEL SHANNON A., LANG ROBERT J., THOMSON MARK W., SIGEL DEBORAH A., WALKEMEYER PHILLIP E., TREASE BRIAN P., MAGLEBY SPENCER P. and HOWELL LARRY L., *J. Mech. Des.*, **135** (2013) 111005.

[37] MOUSANEZHAD DAVOOD, KAMRAVA SOROUSH and VAZIRI ASHKAN, *Sci. Rep.*, **7** (2017) 14792.

[38] DEMAINE ERIK D., DEMAINE MARTIN L., KOSCHITZ DUKS and TACHI TOMOHIRO, *Curved crease folding: a review on art, design and mathematics,* in *Proceedings of the IABSE-IASS Symposium: Taller, Longer, Lighter (IABSE-IASS2011), London, England* (Citeseer) 2011, pp. 20–23.

[39] DIAS MARCELO A., DUDTE LEVI H., MAHADEVAN L. and SANTANGELO CHRISTIAN D., *Phys. Rev. Lett.*, **109** (2012) 114301.

[40] DIAS MARCELO A. and SANTANGELO CHRISTIAN D., *EPL*, **100** (2012) 54005.